Numerical study of winter water formation in the Chukchi Sea: Roles and impacts of coastal polynyas

Yusuke Kawaguchi,[1] Takeshi Tamura,[2,3] Shigeto Nishino,[1] Takashi Kikuchi,[1] Motoyo Itoh,[1] and Humio Mitsudera[4]

Received 18 August 2010; revised 24 March 2011; accepted 26 April 2011; published 28 July 2011.

[1] Winter water formation is examined in the Chukchi Sea for the winters of 1992–2006 using a primitive equation ocean model forced by NCEP wind and surface salinity flux derived from SSM/I thin ice thickness estimates. The model is also forced by an external inflow of 0.8 Sv through the Bering Strait. The model successfully reproduces the oceanic circulation on the Chukchi shelf, thus providing numerous insights into behaviors of salt-enriched water produced on the shelf. The experiments show that under northeasterly winds, northward throughflow across Barrow Canyon is reduced. This results in salinity buildup under freezing conditions and ultimately in greater enhancement of salinity of the waters carried into the Arctic Basin. The flow and salinity enhancement of the flow through Herald Canyon is less extreme but more steady than through Barrow Canyon. Together with moored salinity in the Bering Strait, the model results estimate the actual salinity to be 32.9 ± 0.8 psu and 32.7 ± 0.3 psu, respectively, for waters moving through the Barrow and Herald Canyons. Both estimates are less than 33.1 psu that is typically observed for the cold halostad layer in the Canada Basin, suggesting the importance of diapycnal mixing with saltier Atlantic origin water.

Citation: Kawaguchi, Y., T. Tamura, S. Nishino, T. Kikuchi, M. Itoh, and H. Mitsudera (2011), Numerical study of winter water formation in the Chukchi Sea: Roles and impacts of coastal polynyas, *J. Geophys. Res.*, *116*, C07025, doi:10.1029/2010JC006606.

1. Introduction

[2] In the Arctic Ocean, the cold halocline layer between depths of 50 and 200 m acts as an effective barrier between relatively fresh surface mixed layer and the warmer and saltier Atlantic layer [*Aagaard et al.*, 1981]. In the absence of the halocline layer, the mixed layer receives the upward heat flux from the underlying warm water, and this could promote melting of the sea ice cover. One principal mechanism for halocline formation is ice production and accompanying brine rejection over the shallow continental shelves; these processes create cold and saline waters that descend across the shelf slope and ventilate the cold halocline layer as well as deep waters of the Arctic Ocean. In addition, the salinity-enhanced winter water on the shelf is known to deliver a considerable amount of nutrients to subsurface layer in the Arctic Basins [*Walsh et al.*, 1989].

[3] Previous studies [e.g., *Winsor and Björk*, 2000] have identified the Chukchi shelf as one of the most productive areas for cold and saline shelf waters in the Arctic Ocean because of frequent polynya occurrence. *Shimada et al.* [2005] examined the varieties and spatial distribution of Pacific and Eastern Arctic origin halocline waters in the Canada Basin based on hydrographical data. They insisted that the halocline structure in the Canada Basin differs from that found in the Eastern Arctic because it includes fresh Pacific Winter Water (hereafter referred to as PWW) and forms a "cold halostad layer" which has relatively weak stratification in the halocline layer and has nearly homogeneous temperature close to freezing point. *Shimada et al.* [2005] also argued that the PWW, and consequently the cold halostad layer, has an nonuniform spatial structure that varies depending on the pathways and source waters. This PWW that moves along the eastern Chukchi shelf exhibits a wide range of salinities because of occasional salt production, and subsequently, it spreads along the northern Chukchi slope and into the southern Canada Basin. In contrast, in the region downstream of the Herald Canyon, the PWW intrusion from the western Chukchi Sea results in a narrow salinity range and restricted ventilation. The present study aims to reveal and quantify the spatial variation of PWW distribution indicated from hydrographical observation such as *Shimada et al.* [2005].

[4] *Weingartner et al.* [1998, 2005] analyzed the hydrographical measurements obtained from moorings at several locations on the Chukchi shelf. They found outbreaks of cold and hypersaline water (>34.0 psu) that were capable of

[1]Japan Agency for Marine-Earth Science and Technology, Yokosuka, Japan.
[2]Antarctic Climate and Ecosystem Cooperative Research Center, University of Tasmania, Hobart, Tasmania, Australia.
[3]National Institute of Polar Research, Tachikawa, Japan.
[4]Institute of Low Temperature Science, Hokkaido University, Sapporo, Japan.

0148-0227/11/2010JC006606

ventilating the lower halocline layer as well as the deep Canada Basin, and suggested that these were attributable to considerable ice formation associated with the polynya activity between Pt. Barrow and Cape Lisburne (hereafter referred to as Barrow coastal polynya).

[5] *Winsor and Björk* [2000] calculated ice productions for 28 Arctic coastal polynyas between 1958 and 1997 using an analytical polynya model that gives offshore polynya width (polynya area per coastal length) from the offshore wind speed and air temperature [*Pease*, 1987]. They also estimated the volume of salinity-enhanced water produced in the Chukchi Sea as a consequence of polynya activity. In their estimation, the Pacific origin water, approximately 31.6 psu in September, can be enhanced up to 33.5–36 psu (35–42 psu if the advection of 2 cm s^{-1} is not incorporated), corresponding to a density between the lower halocline and the deep Atlantic water layers in the Canada Basin. *Winsor and Chapman* [2002] examined dense water formation for the Barrow coastal polynya using a three-dimensional oceanic model and they determined the salinity (density) associated with baroclinic eddies generated along the polynya edge. They showed that the maximum salinity anomaly is typically 1.0–1.5 psu beneath the polynya (depending on the forcing data set used) and also discussed the interannual variability of the production volume of the water. *Martin et al.* [2004] calculated ice formation volume for the same polynya between 1990 and 2001, based on heat flux calculations at ocean surface with Special Sensor Microwave Imagery (SSM/I) derived sea ice thickness. They compared the ice volume derived using the SSM/I algorithm (see *Martin et al.* [2004] for detail) with that obtained by *Winsor and Chapman* [2002] that used the *Pease*'s [1987] analytical model. They then showed a significant difference between the two estimates.

[6] Most previous studies have focused on dense water volume and its maximum salinity produced upon the Chukchi shelf. However, hardly any studies have addressed the amount of water entering the Canada Basin and actually contributing to the ventilation at the cold halocline layer. This problem may significantly depend on how well oceanic circulation and also surface salinity flux, because of sea ice production, are reproduced. Furthermore, the salt-enriched water is very limited; it passes the shelfbreak only through a few channels, e.g., the Barrow and Herald Canyons. Therefore, local current velocity and detailed bathymetry is essential to quantitatively estimate volume flux and its salinity in the cold halocline layer.

[7] Climate changes in the western Arctic Ocean are dominated by pronounced summer ice reduction [e.g., *Shimada et al.*, 2006; *Stroeve et al.*, 2007]. Since distribution of multiyear ice in autumn can significantly affect ice production the following winter, summer ice retreat tends to increase winter ice production. Furthermore, recent changes in atmospheric wind system, such as the Arctic Oscillation, primarily determine ice drift velocity [*Rigor et al.*, 2002] and consequently the amount of ice outflow from the region [*Kwok*, 2008]. This may also influence polynya activity because local wind direction over coastal region determines polynya area and its frequency [*Kawaguchi et al.*, 2010].

[8] In the present paper, we conduct a three-dimensional simulation for winters 1992–2006 at a fine spatial resolution that can reproduce the detailed ocean circulation on the Chukchi shelf. Because the model is also forced by the surface salinity fluxes derived from SSM/I brightness temperature (T_{bs}) [*Tamura et al.*, 2007, 2008; *Tamura and Ohshima*, 2011], it is capable of showing both the processes for formation and transportation of salt-enriched water. We then calculate the volume flux and its annual variability ventilating the winter water layer in the western Arctic Ocean. Furthermore, sea ice production data is analyzed and discussed from the perspective of horizontal distribution, interannual and interseasonal variability for the 1992–2006 period.

[9] In section 2, the oceanic model is described along with the SSM/I thin ice thickness algorithm. Then, the sea ice production derived from the algorithm is analyzed in section 3. The model results are presented in sections 4–7. First, the simulated circulation is verified in comparison with mooring measurements in section 4. Then, dense water formation for the 1993 and 1994 winters are described in section 5, where these winters are representative for frequent and less frequent polynya occurrence, respectively. In section 6, water volume of the ventilated PWW is quantitatively discussed. In section 7, practical salinity value to ventilate the cold halocline layer is discussed. Finally, section 8 summarizes the present study.

2. Model and Data Descriptions

2.1. Oceanic Model

[10] In this study, we adopted the Princeton Ocean Model (POM), a free surface, hydrostatic, primitive equation model [*Blumberg and Mellor*, 1987]. This model uses stretched, terrain-following coordinates in the vertical and orthogonal curvilinear coordinates in the horizontal. For the present study, the model gives solutions for 11 sigma levels, located at relative depths of 0, 0.1, 0.2, 0.3, 0.5, 0.7, 0.9, 0.95, 0.988, 0.99, and 1.0, where 0 and 1.0 denote the bottom and the surface, respectively. The POM solves the standard Boussinesq momentum, temperature, salinity, and continuity equations. The model domain covers the Chukchi shelf, 175–215°E (145°W) and 65–75°N (Figure 1), which extends westward up to the west of Wrangel Island in the East Siberian Sea, eastward along the entire Beaufort shelf, southward to the Bering Strait, and northward to the middle of the Chukchi Borderland. Choice of the model domain is similar to that by *Winsor and Chapman* [2004], except that the northward extension of 75°N is less broad than their configuration, 78°N. The rotational Coriolis parameters are calculated depending on the local grids between 65–75°N, corresponding to $1.3–1.4 \times 10^{-4}$ s^{-1}.

[11] In the model, the horizontal resolution is 1/20 and 3/20° in latitude and longitude, respectively, corresponding to approximately 5.5 km and 4–7 km; this is sufficiently fine to resolve detailed structures of the current steered by the bathymetry, including intensified velocity at both the Barrow and Herald Canyons. The model domain has three open boundaries on the north, east, and west edges, at which radiation open boundary condition is applied for the lateral boundary (G. L. Mellor, Users guide for a three-dimensional, primitive equation, numerical ocean model, http://www.aos.princeton.edu/WWWPUBLIC/htdocs.pom/, 2004). The bathymetry is taken from the International Bathymetry Chart of the Arctic Ocean (IBCAO) with a

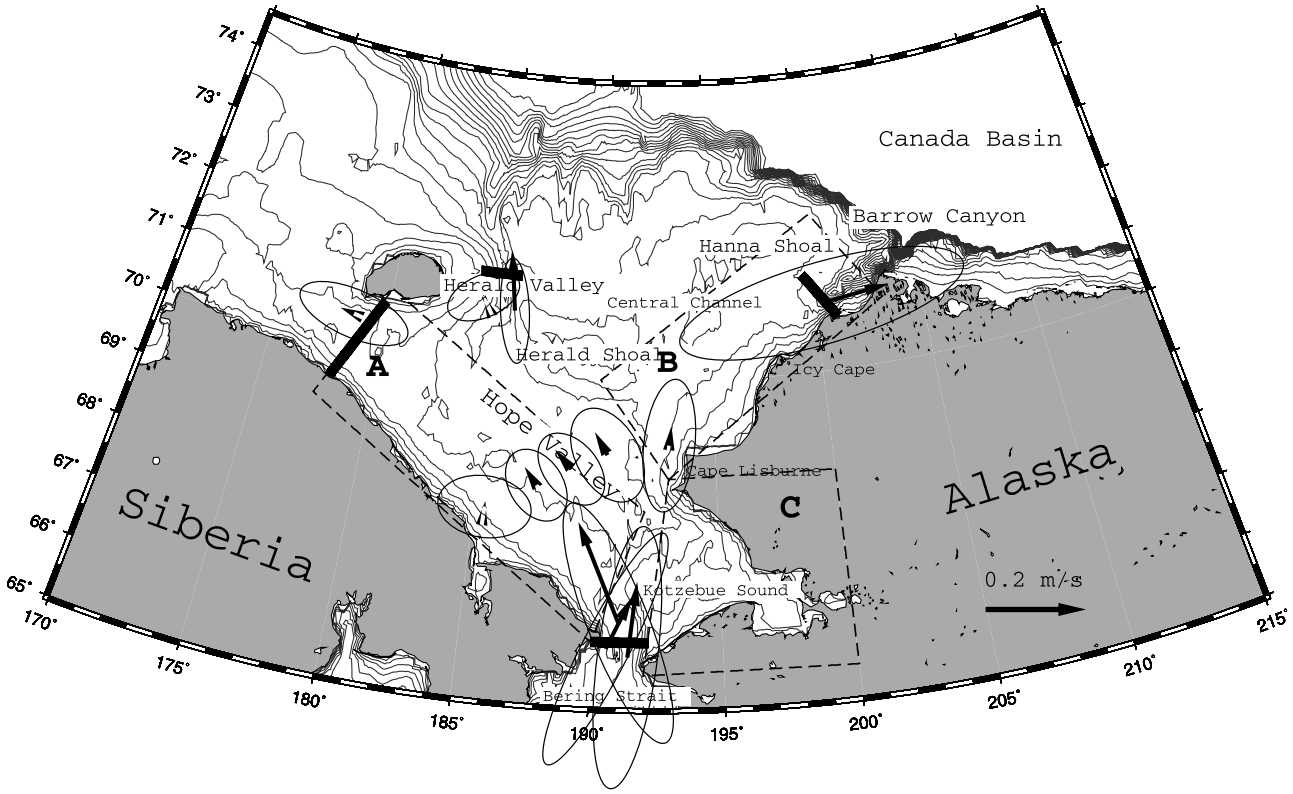

Figure 1. A plan view of model domain. Regions enclosed by dashed lines denote East Siberian (region A), Barrow (region B), and Kotzebue (region C) coastal polynyas. Moored current velocities are also plotted in vector, which are averages between September 1990 and September 1991. See the main text and also *Woodgate et al.* [2005c] for detailed information about the mooring systems.

spatial resolution of 2.5 km, which is interpolated to fit the model grid with a Gaussian filter of 10 km in effective length. The bottom topography is cut off such that it is flat for regions deeper than 300 m.

[12] In this study, a series of simulations are performed for winters of 1992–2006, where each run begins on November 1 and lasts until May 31. The numerical calculation begins from rest with spatially homogeneous salinity and temperature, respectively set to be 32.0 psu and −0.5°C. In the present study, the salinity anomaly from the initial value indicates salinity enhancement from ice production, and then, the temperature is fixed at −0.5°C. The model is forced with daily surface salinity flux estimated from the SSM/I thin ice thickness algorithm and heat flux calculation [*Tamura and Ohshima*, 2011], whose details are described in section 2.2. In this study, we do not couple an explicit ice model with the oceanic model because it is uncertain whether it correctly predicts the distributions of ice concentration and ice thickness for each winter.

[13] We force the model based on a following formulation, $C_d U_{10}|U_{10}|$, where U_{10} is daily 10 m winds, provided from National Centers for Environmental Prediction (NCEP), and $C_d = 0.0015$ (kg m^{-3}). The surface salinity flux (F_s) is calculated after conversion from the ice production rate V_i by the following equation [cf. *Cavalieri and Martin*, 1994; *Martin et al.*, 1998]:

$$F_s = \rho_i V_i (S_w - S_i) \times 10^{-3}, \quad (1)$$

where S_w and S_i are the salinity of seawater and sea ice, respectively, and they are set as $S_i = S_w \times 0.31$ [*Martin and Kaufman*, 1981], where $S_w = 32.0$ psu. The model is also forced by the inflow that is externally imposed at the southern boundary of 189–191°E (169–171°W). The external inflow is here given to be 0.8 Sv, so that it is roughly consistent with the in situ estimation provided by *Woodgate et al.* [2005b, 2005c]; the effect of its variation on the dense water formation is examined in section 6.3.

2.2. Surface Salinity Flux From SSM/I Thin Ice Thickness Algorithm

[14] The surface salinity flux calculated from sea ice production is based on the heat budget calculation using the SSM/I thin ice algorithm developed by *Tamura and Ohshima* [2011; see also *Tamura et al.*, 2007, 2008]. Their estimation used the Equal Area Scalable Earth-Grid (EASE-Grid) SSM/I brightness temperature T_{bs} that were provided by the National Snow and Ice Data Center (NSIDC). The data set is in turn interpolated to match the Chukchi regional simulation performed in this study. *Tamura and Ohshima* [2011] estimated sea ice thickness from the SSM/I T_{bs} and validated with thicknesses derived from thermal infrared Advanced Very High Resolution Radiometer (AVHRR) data [*Yu and Rothrock*, 1996; *Drucker et al.*, 2003; *Tamura et al.*, 2006]; the thickness was then applied to calculate the heat flux at the sea ice surface conducted through the ice interior. Air and dew

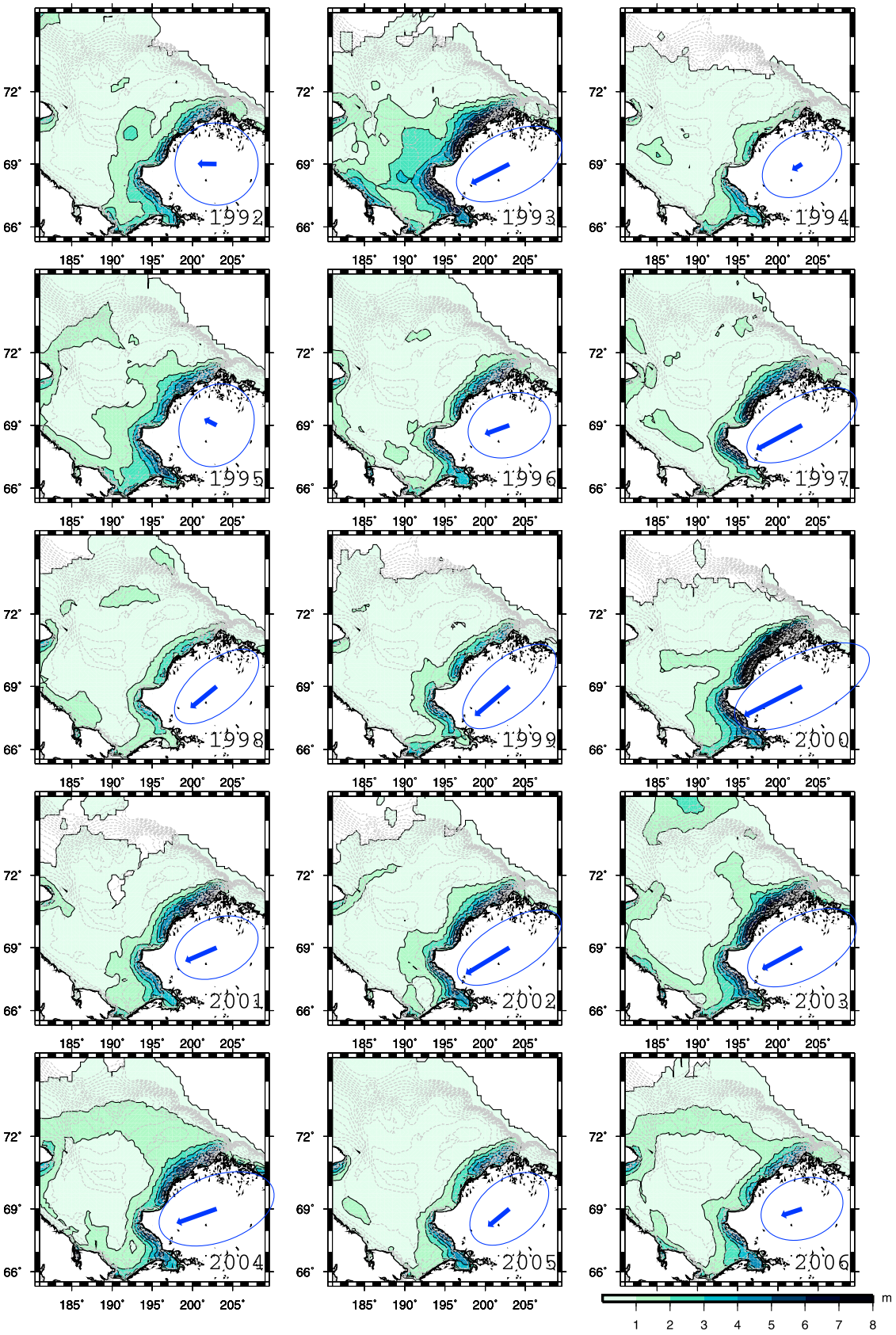

Figure 2. Cumulative ice production (in meter) between November and March in 1992–2006. Vectors represent an average of 10 m wind velocity for the period in the northeastern Chukchi Sea, where maximum strength is approximately 4 m s^{-1} in the winter of 2000.

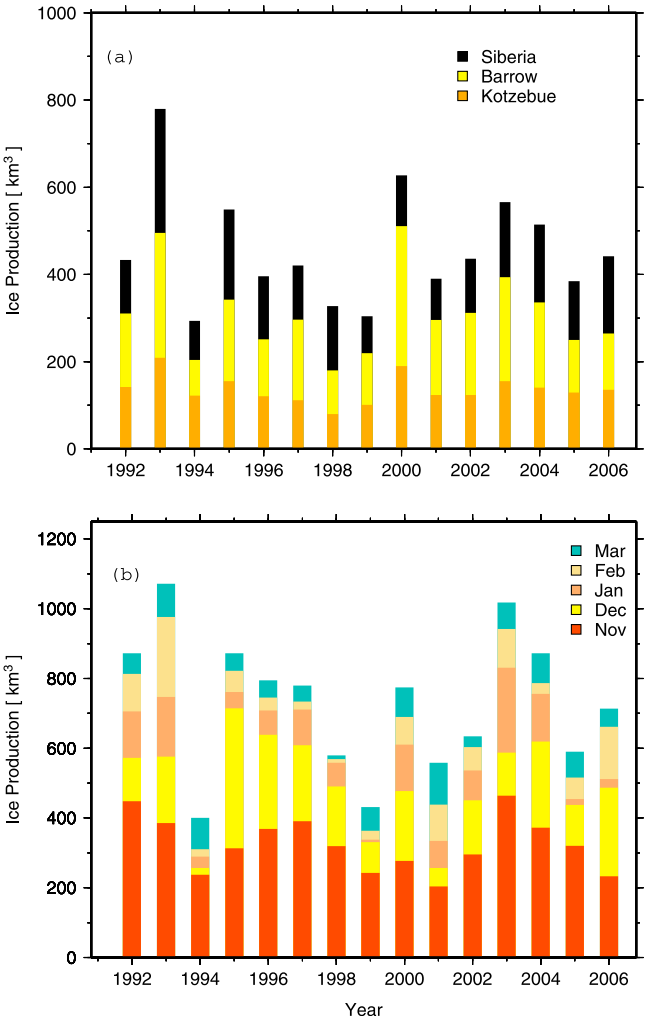

Figure 3. (a) Cumulative ice production for respective coastal polynyas: East Siberian, Barrow, and Kotzebue coastal polynyas. (b) Cumulative ice production for each month, which is accumulated over the entire Chukchi Shelf.

point temperatures (both at a height of 2 m), and the 10 m wind and mean sea level pressure (SLP) are also used in heat budget calculation, which are taken from NCEP2 (National Centers for Environmental Prediction/Department of Energy Reanalysis) data.

[15] We should note that there is a possibility that in the early freezing period (e.g. November), heat loss in the thin ice region could be used for the cooling of surface water instead of being used for sea ice production; this may lead to overestimation of sea ice production. However, in the above estimation of sea ice production and salt flux, ice production only occurred in thin ice region (<0.15 m) whose ice concentration is more than 30%, where Bootstrap sea ice concentration [*Comiso et al.*, 1984; *Comiso*, 1986] provided by NSIDC is used. This conservative threshold of 30% ice concentration is considered to be enough to assume that the water temperature under the ice is at the freezing point (271 K), leading to low probability of overestimation of ice production. Please refer to *Tamura et al.* [2007, 2008] and *Tamura and Ohshima* [2011] for detailed descriptions of the ice thickness estimation, heat budget calculation, and sea ice production at the ocean surface.

3. Analyses of Sea Ice Production Using SSM/I Algorithm

[16] We describe characteristics of sea ice production derived using the SSM/I algorithm from the viewpoint of spatial distribution, its interannual and interseasonal variations.

3.1. Spatial Distribution

[17] Figure 2 shows horizontal distribution of cumulative ice production for each winter during 1992–2006 over the Chukchi shelf. The most prominent feature is extensive sea ice formation confined within narrow coastal regions. Figure 2 exhibits that the polynya activity in this regions is highly variable over the years. Another feature is substantial ice production over the broad shelf region in the Chukchi Sea, equivalent to 0.5–1 m as an accumulated value, indicating seasonal ice formation rather than spatially confined polynya activity.

[18] Figure 3a shows cumulative ice production for three coastal polynyas in the Chukchi Sea: a polynya between Pt. Barrow and Cape Lisburne (Barrow coastal polynya as defined previously), a polynya in the Kotzebue Sound (Kotzebue polynya) in the northeast part of the Bering Strait, and a polynya along the East Siberian coast (East Siberian coastal polynya).

3.1.1. Barrow Coastal Polynya

[19] The Barrow coastal polynya exhibits the highest ice production, 175 km^3 on average between 1992 and 2006, and its annual variability is consistent with *Martin et al.* [2004] (hereafter referred to as M04). Ice production is highest in 2000 and lowest in 1994. M04 reported the integrated ice volume to be 70 km^3 on average, which is less than half of our estimate. On the other hand, *Cavalieri and Martin* [1994] (hereafter referred to as CM94) reported 165 km^3 ice volume, which is relatively close to our value. The considerable difference between our and M04's estimate is probably due to duration used in the calculation: in our and CM94's estimation, ice production is assumed to start as the sea ice concentration (SIC) exceeds a threshold in the early winter; we consider the SIC threshold to be 30% (see section 2.2), whereas CM94 used 15% and 30%. M04 manually determined the onset of ice production because they mainly focused on the polynya activity of the Barrow coastal polynya.

3.1.2. Kotzebue Polynya

[20] The Kotzebue polynya exhibits the second-highest ice production, and it is comparable to that in the Barrow polynya in our estimate. The polynya occurrence in the Kotzebue Sound is not very sensitive to the northeasterly wind (Figure 4a), unlike the Barrow polynya, but it exhibits sufficient polynya occurrences. This may be because of the complex geometry adjacent to the Kotzebue Sound, leading to an offshore wind component for various wind directions, which in turn results in a favorable condition for polynya formation.

3.1.3. East Siberian Coastal Polynya

[21] Ice production in the East Siberian coastal polynya is 0.5–2 m per year, which is close to the seasonal ice production observed over the central Chukchi Sea. This implies

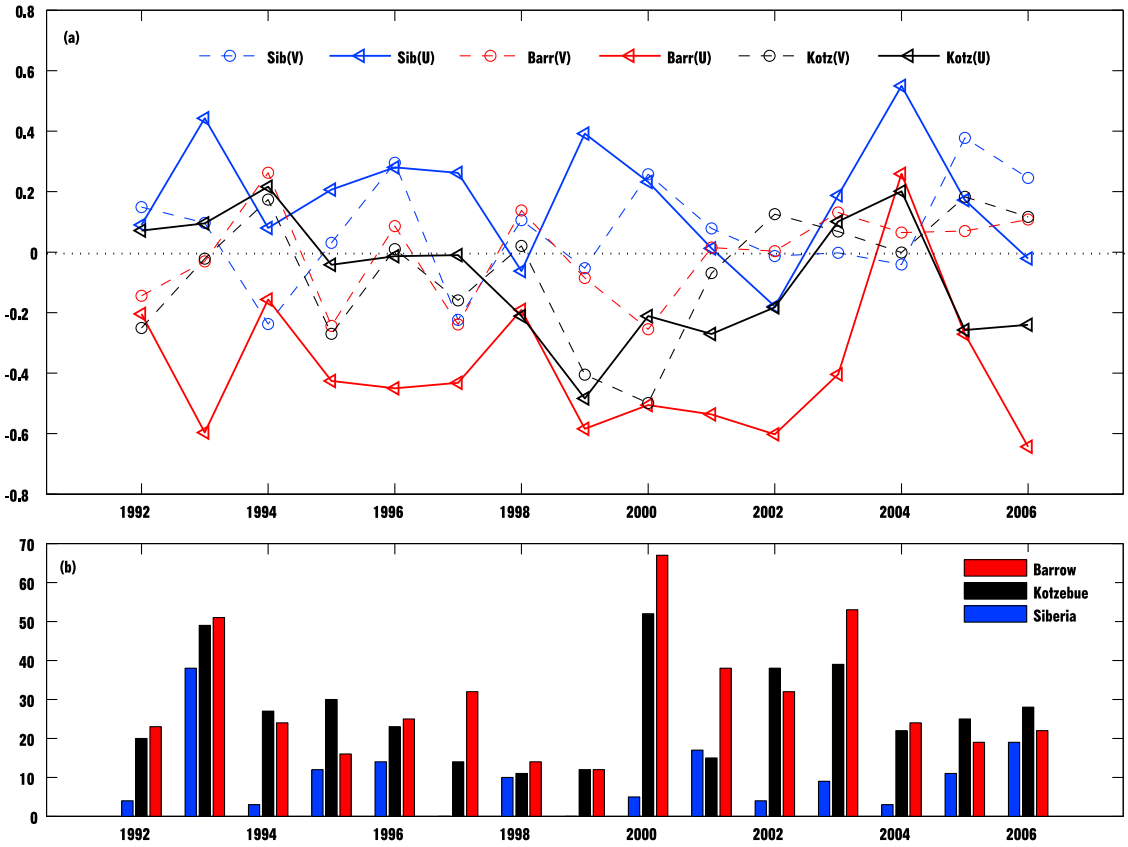

Figure 4. (a) Time series of correlation coefficients between daily wind velocity and thin ice area, where *U* and *V* are wind components for eastward and northward direction, respectively. (b) Occurrence (days) of thin ice event in each polynya region. It is counted when thin ice area is greater than 20,000 km^2, corresponding to 50 km polynya width supposing 400 km coastline. Note that ice-free region before 20th December is not included in the calculation.

that the East Siberian polynya occurs infrequently relative to the other two polynyas (Figure 4b). As an exception, it was very active in winter 1993 when the integrated ice volume reached 210 km^3; this was comparable to volumes of 286 and 284 km^3 for the Barrow and Kotzebue polynyas, respectively.

3.2. Interannual and Interseasonal Variations

[22] Figure 3b shows interannual and interseasonal variability of ice production integrated over the entire Chukchi shelf. Note that it includes ice production in the remainder of the Chukchi shelf besides the coastal polynyas. The annual variability of ice production is generally consistent with the sum of that in each polynya (Figure 3a), the average being 730 km^3 with the variation of ~30%. Accumulated ice volume is similar to CM04's estimate; it is 850 and 680 km^3, respectively, for early and late start days on the basis of SIC thresholds of 15 and 30%. In contrast, it is greater by a factor of 10 as compared to analytical polynya models, such as those by *Winsor and Björk* [2000] and *Winsor and Chapman* [2002]. From the viewpoint of ice volume flux exported through Fram Strait, ~3400 km^3 [*Rothrock et al.*, 2000], it is equivalent to ~20%.

[23] Figure 3 also shows that most ice production occurs in early winter, i.e., November and December. This is because numerous amount of frazil ice is formed over the shelf region immediately after the water column reaches the freezing temperature. The ice production is highest in November and second highest in December, when the respective averages for the 15 winters are 325 km^3 and 176 km^3, corresponding to 44% and 24% of the total ice production averaged for the winters. In M04's estimation, it is highest in December and second highest in November; this is probably because they only consider ice production occurred in the Barrow coastal polynya. Additionally, they did not include ice production before the coastal area was completely surrounded by the first-year ice, thus neglecting the growth of ambient sea ice. While ice production is largely stable in early winter, it is very variable during the midwinter between January and March. The average value for the three months is 77 km^3 with 65% (50 km^3) standard deviation. This indicates that polynya occurrence is quite sensitive to various factors such as wind velocity, oceanic current, and ice concentration.

3.3. Relationship Between Polynya Activity and Atmospheric Circulation

[24] Here, relationship between the frequency of polynya occurrence and atmospheric wind pattern is discussed. Figure 2 depicts surface wind vector integrated over the northern Chukchi Sea (69–72°N, 185–205°E). Figure 2 illustrates that the Barrow coastal polynya appears to open

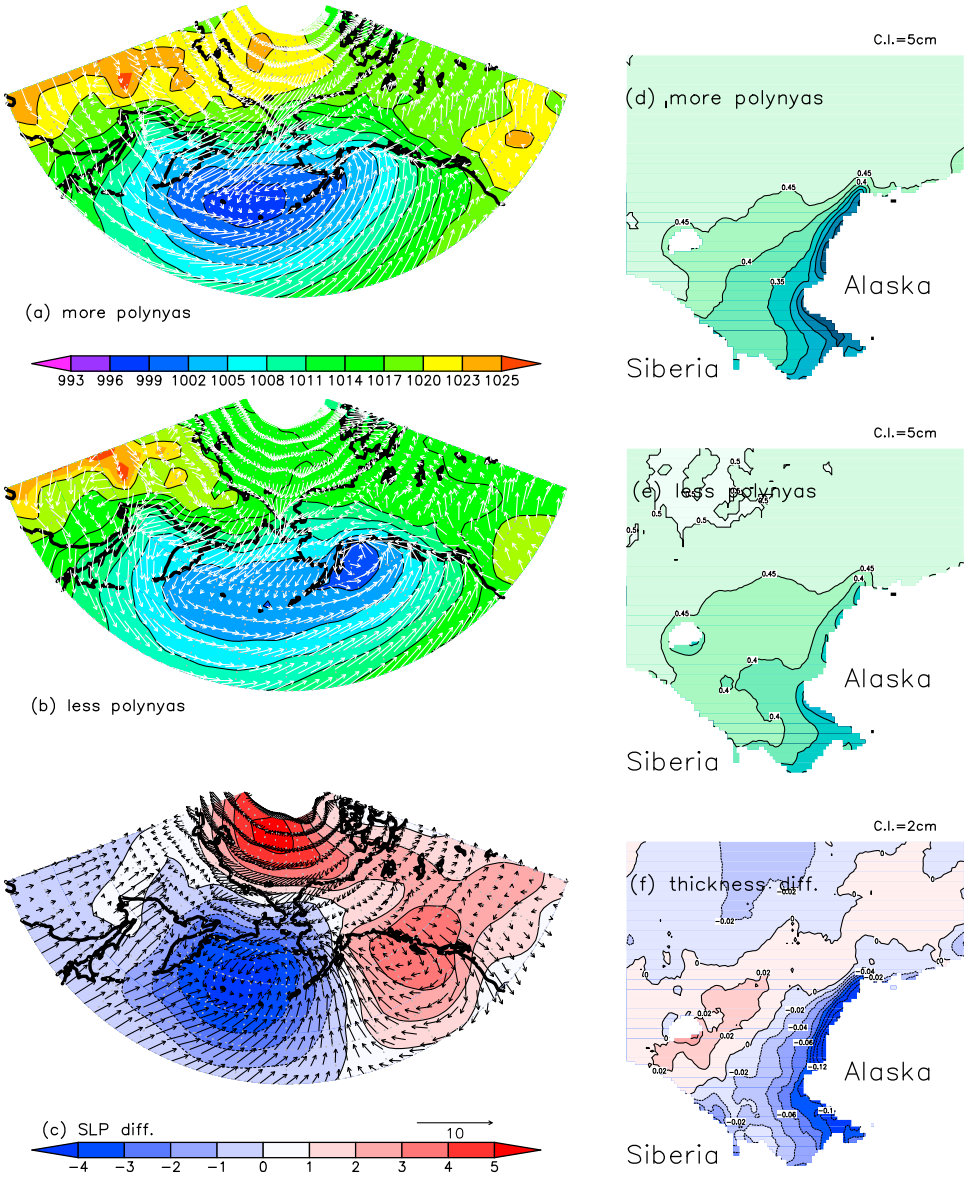

Figure 5. Mean SLP and 10 m wind for groups with (a) frequent and (b) infrequent polynya occurrences: 1993, 2000, and 2003, and 1994, 1998, 1999, 2005, and 2006, respectively. (c) Differences of SLP and wind velocity between the two groups. (d and e) Ice thicknesses averaged over respective groups of frequent and infrequent polynya years. (f) Ice thickness difference between the two groups, where values in Figure 5d are subtracted by those in Figure 5e.

favorably when northeasterly wind blows strongly over the region, which is intuitively consistent with the correlations shown in Figure 4a. For example, such wind component is quite large in winters 1993, 2000, and 2003 (3–4 m s^{-1}), when coastal polynyas are formed frequently (Figure 4b), and thus, the accumulated ice production volume during a winter is considerably large; it is equivalent to 8–10 m per unit area for the winter. In contrast, wind velocities are lower (<2 m s^{-1}) for winters 1994, 1998, 2005, and 2006, when the annual accumulated volume is reduced to between 1 and 4 m per unit area.

[25] To clarify the relationship between wind pattern and polynya formation, we conducted a composite analysis in terms of SLP pattern over the north Pacific–central Arctic Oceans, where they are classified into two groups of high and low ice production based on its statistical average regarding the Barrow polynya. The consequence shows that winters (1993, 2000, 2003) are highly ice productive, while winters (1994, 1998, 1999, 2005, 2006) have low ice production (Figures 5d, 5e, and 5f), where members of each group are selected based on whether deviation from the average is greater than a standard deviation 6.7×10^{10} km^3, 38% of the 15 years average, or not.

[26] Figure 5 plots results of the analysis, where surface wind vectors overlaid with the SLP contours are plotted for each group. Comparison between the two groups shows a significant difference in the synoptic atmospheric circulation. In both groups, the Aleutian low-pressure and Beaufort high-pressure systems are commonly established over the North Pacific and the Western Arctic Oceans, respectively.

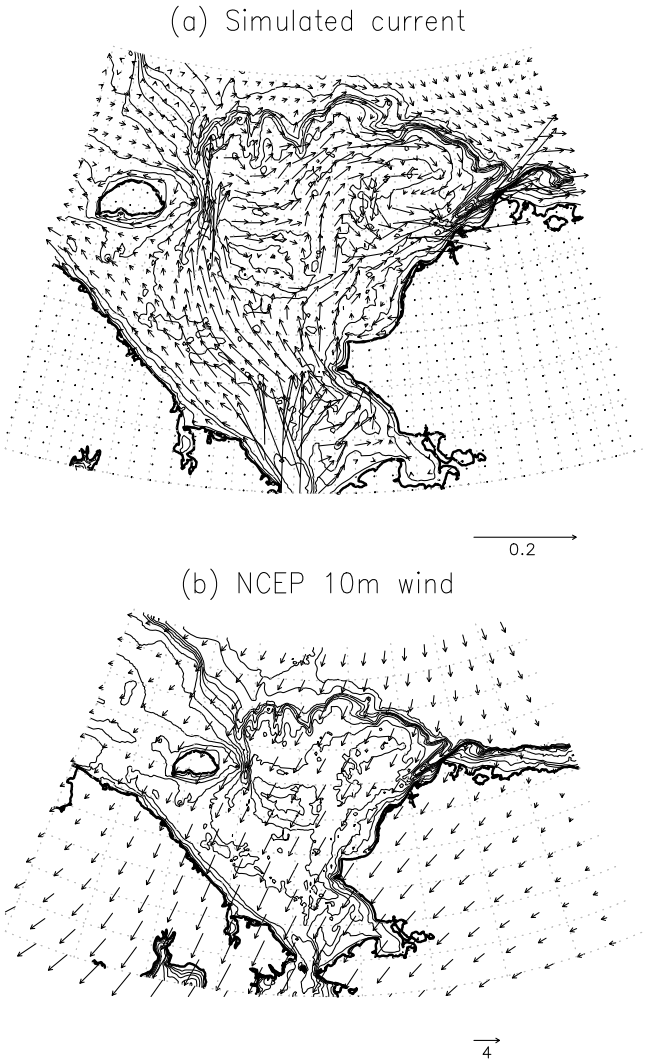

Figure 6. (a) Simulated current velocity (m s^{-1}), averaged from November to May in 1990/1991, and (b) NCEP wind vectors (m s^{-1}) at 10 m height that are averages for the same period.

However, there are substantial differences between the two cases. For example, it is found in the intensity of Beaufort high-pressure system, and additionally, it is on the location of Aleutian low-pressure system (Figure 5c). That is, in the frequent polynya occurrence group, the Beaufort high pressure tends to be further intensified on its center core, and additionally, the Aleutian low pressure system is located further west relative to the other group. Such synoptic-scale atmospheric patterns may induce the stronger SLP contrast between the north and the south of the Alaskan continent, so that it promotes northeasterly winds, and consequently, results in more frequent polynya occurrence.

4. Reproduction of Oceanic Circulation: Comparison With Multiple Moorings in 1990/1991

[27] To verify the application of the model for the problem of dense water formation in the Chukchi Sea, the simulated current is compared with the mooring observation obtained by the University of Washington. The multiple mooring systems were deployed at approximately 10 m above the seafloor and current velocity was recorded between September 1990 and September 1991; these cover the entire Chukchi shelf and enable the calculation of net fluxes of water volume, heat, and salt (see the paper by *Woodgate et al.* [2005c] for further information).

[28] Figures 1 and 6, and Table 1 show comparisons between observed and modeled current velocities, where the model output is averaged between November 1990 and May 1991. Figures 1 and 6 and Table 1 show that the simulation suitably captures the characteristics of the observed circulation over the Chukchi Sea.

[29] Observed northward flow in the vicinity of the Bering Strait is well reproduced by the model, where the velocities to the east and west (MA1 and MA2) of Diomede Island are calculated to be 24 and 28 cm s^{-1} respectively in the model, similar to the observation of ~29 cm s^{-1} (Table 1). To the north of the Bering Strait, MA3, they are similarly consistent in both magnitude and direction, where the current speeds are roughly 20 cm s^{-1} directed northward with a small westward fraction. With regard to the MC line across the central Chukchi Sea, the intensified northward flow (>20 cm s^{-1}) via the Bering Strait bifurcates into the broad northwestward passage entering the Hope Valley and the relatively narrow branch moving north along the Alaskan coast. For these features, the modeled velocity agrees well with the observed one at MC2, 3, and 4, which are directed northwestward with velocities of 3–5 cm s^{-1}. MC6, located to the west of Pt. Hope, flows northward along the Alaskan coast; it is simulated to have a velocity of 3.1 cm s^{-1}, and this is slightly smaller than the measured magnitude of 4.1 cm s^{-1}.

[30] Because there were no moorings in this year over the Hanna and Herald Shoals and on the northern shelf slope, the model results shown in Figure 6a are also compared with those from a barotropic ocean model [*Winsor and Chapman*, 2004]. The mean ocean circulation calculated for 1990/1991 winter resembles their circulation that is forced merely by a steady northward inflow of 0.8 Sv from the Bering Strait [*Winsor and Chapman*, 2004, Figure 3]. The broad northward flow via the Bering Strait trifurcates into three major branches to the west of Pt. Hope as mentioned. Subsequently, the eastern passage moves northeastward along the Alaskan coast (this current is called the Alaskan Coastal Current, or simply ACC) and directly drains into the Barrow Canyon. The broadest branch moving through the Hope Valley is intensified as it passes through the Herald Valley. Some of the Pacific origin water via the Herald Canyon escapes by descending across the slope into the west of the Chukchi Borderland, and then moves eastward along the shelf edge. The remaining branch moves along the middle pathway between the Herald and the Hanna Shoals, which is called the Central Channel by *Weingartner et al.* [1998], and some of them join the eastward flows from the Herald Canyon to the north of the Hanna Shoal.

[31] According to the moored measurement at MF1, to the west of the Herald Canyon, the northward flow is far less intensified relative to the other side of MF2 (see Table 1). In the model, the current strength is 3.6 cm s^{-1} at the western side; this is smaller than the strength of 11 cm s^{-1} at the eastern side, although it is still larger than the measured

Table 1. Observed and Simulated Current Velocity at Each Mooring Location[a]

Mooring Identifier	Location	Longitude (W), Latitude (N)	Observed Magnitude (cm s^{-1})	Direction (deg)	Modeled Magnitude (cm s^{-1})	Direction (deg)
MA1	West Bering Strait	169°25.7′, 65°54.0′	29	27	24	24
MA2	East Bering Strait	168°35.2′, 65°46.5′	29	8	28	2
MA3	North Bering Strait	168°57.9′, 66°17.6′	22	338	20	331
MC1	West Central Channel	174°33.2′, 67°56.9′	1.2	9	3.1	318
MC2	Central Channel	172°29.8′, 68°20.5′	4.5	327	5.4	307
MC3	Central Channel	171°4.4′, 68°36.7′	5.2	320	5.3	309
MC4	Central Channel	169°35.6′, 68°51.4′	5.4	331	3.3	334
MC6	East Central Channel	166°57.3′, 69°1.1′	4.1	6	3.1	7
ME2	North Long Strait	181°33.1′, 70°29.7′	3.1	294	2.1	271
MF1	West Herald Valley	175°43.9′, 71°6.9′	0.4	337	3.6	32
MF2	East Herald Valley	174°11.2′, 70°57.8′	12	358	11	1
MK1	Barrow Canyon	159°41.9′, 71°2.0′	14	74	18	59

[a]The values for the observed current are taken from the paper by *Woodgate et al.* [2005c]. The model speed and direction are from the nearest grid points encompassing the mooring positions.

speed of 0.4 cm s^{-1}. This is probably because the velocity at the west is affected by the eastside current in the model owing to the difficulty in fully resolving the velocity in such a narrow strait.

[32] In the Barrow Canyon, corresponding to MK1 in the moorings, there is a slight difference in magnitude between the model and observed velocities. Both the records show a topographically steered northeastward velocity; it has a magnitude of 18 cm s^{-1} in the model, which is larger than the velocity of 14.4 cm s^{-1} obtained from the in situ measurement. This difference can be explained by the fact that our model underestimates the reverse current from the Canada Basin that is principally induced by the easterly wind [*Winsor and Chapman*, 2004], which is frequently observed from October to March in the winter of 1990/1991 [*Woodgate et al.*, 2005c, Figure 10]. The underestimation of the reverse current velocity may be because our model does not fully incorporate basin-scale circulations such as the anticyclonic Beaufort Gyre, which is expected to promote the southwestward up-canyon events. In our calculation, the initial salinity distribution is assumed to be homogeneous, and therefore, the Atlantic deep water uptaken from the basin does not have any net influence on the salinity estimation.

[33] Finally, we discuss the volume flux via the Long Strait. Our model simulates the magnitude of the westward velocity there to be 2.1 cm s^{-1}, which is similar to the in situ measurement of 3.1 cm s^{-1} at ME2. The net transport via the channel is 0.03 ± 0.06 Sv, which is negligible as compared to the total volume of ~0.7 Sv through the Bering Strait.

[34] The winter of 1990/1991 is considered to be a typical winter from the viewpoint of wind pattern (Figure 6b). In this winter, northeasterly wind blows with a strength of ~3 m s^{-1} on average. Then, the external inflow of 0.8 Sv from the southern boundary is weakened by the northeasterly wind, being roughly 0.65 Sv when it passes via the Bering Strait. It then moves across the shelfbreak with volume fluxes of 0.40 and 0.25 Sv via the Barrow and Herald Valleys, respectively.

[35] In conclusion, our model reproduces the oceanic circulation in the Chukchi Sea, and it is generally consistent with the in situ measurements and another numerical study with a barotropic model.

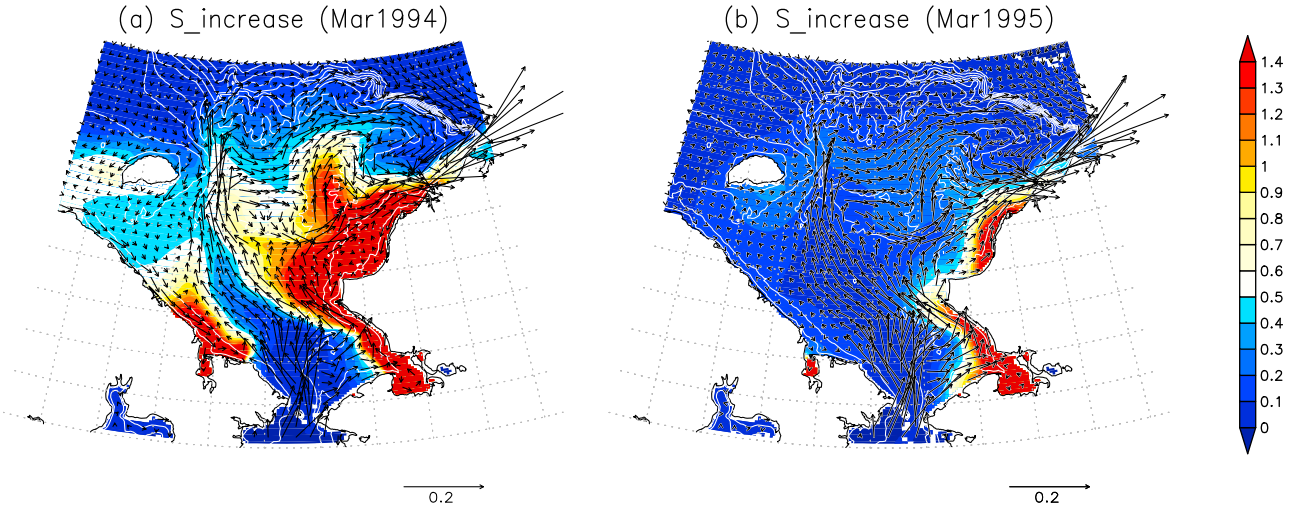

Figure 7. Salinity increment from initial value (psu) in March (a) 1994 and (b) 1995, which are vertical averages at the end of respective months. Current vectors (m s^{-1}) superimposed are averages for each month.

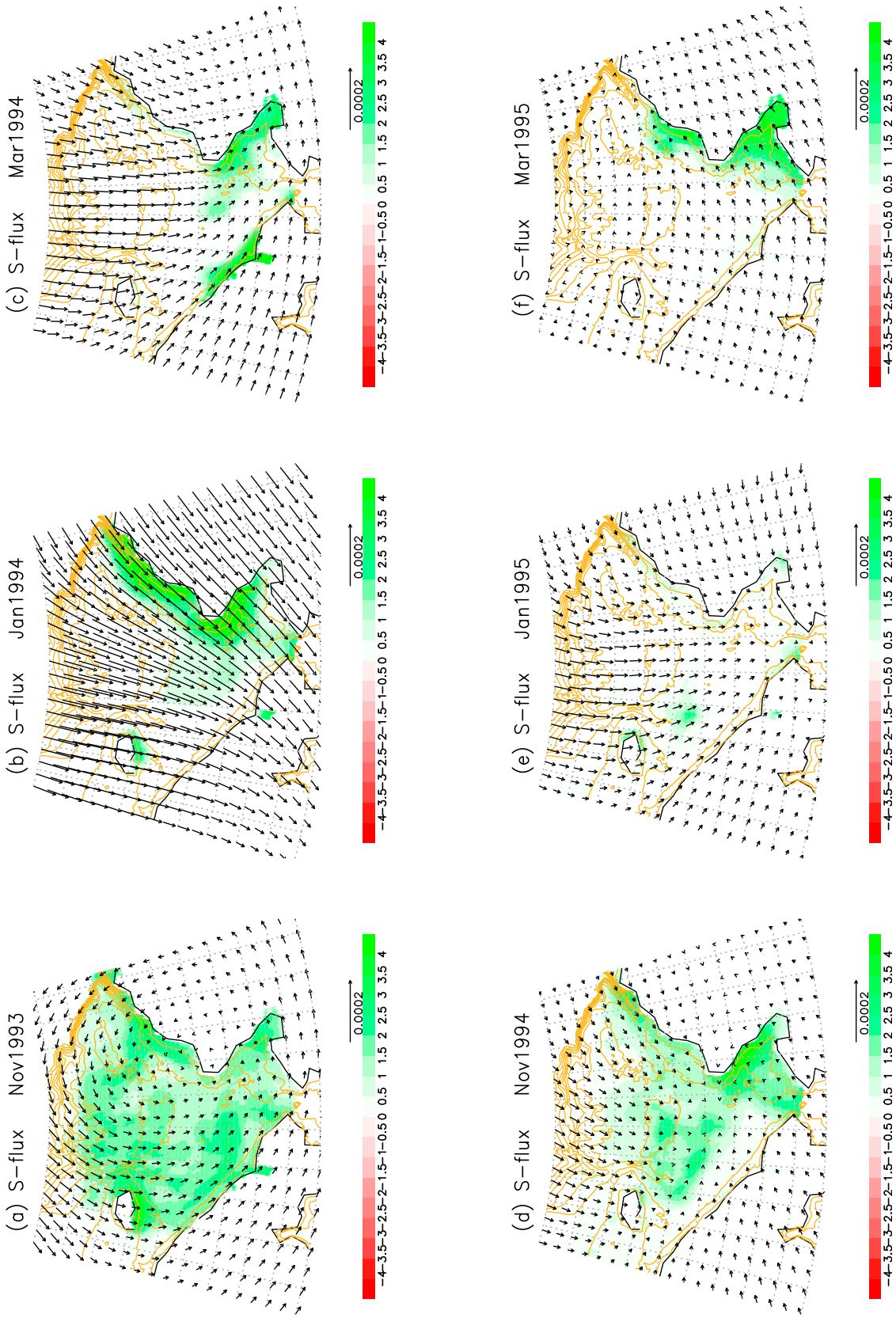

Figure 8. Salinity flux ($\times 10^{-5}$ kg m s^{-1}) averaged for each month in (a–c) 1993/1994 and (d–f) 1994/1995 winters, where surface wind stress ($\times 10^{3}$ Pa) is also superimposed.

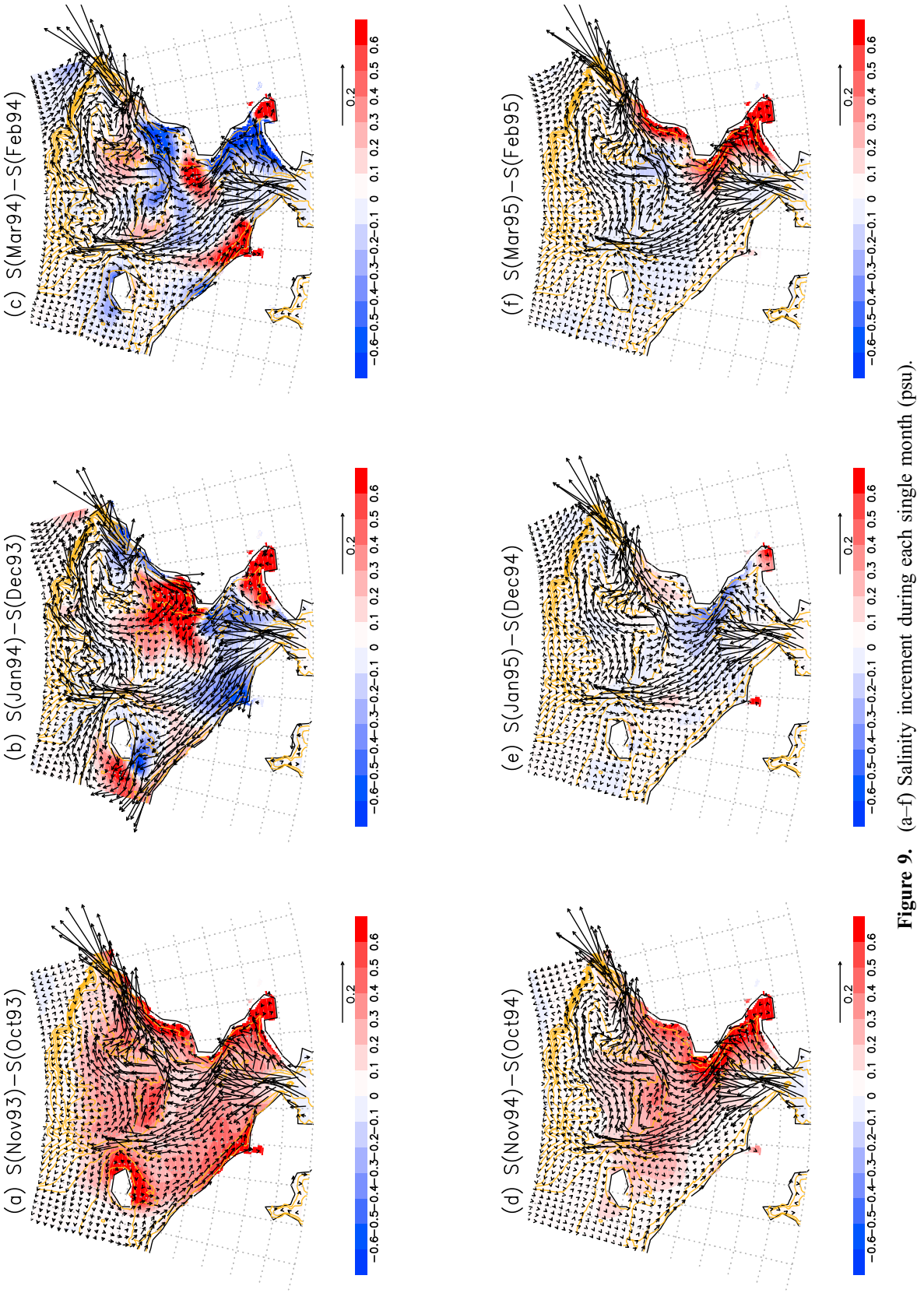

Figure 9. (a–f) Salinity increment during each single month (psu).

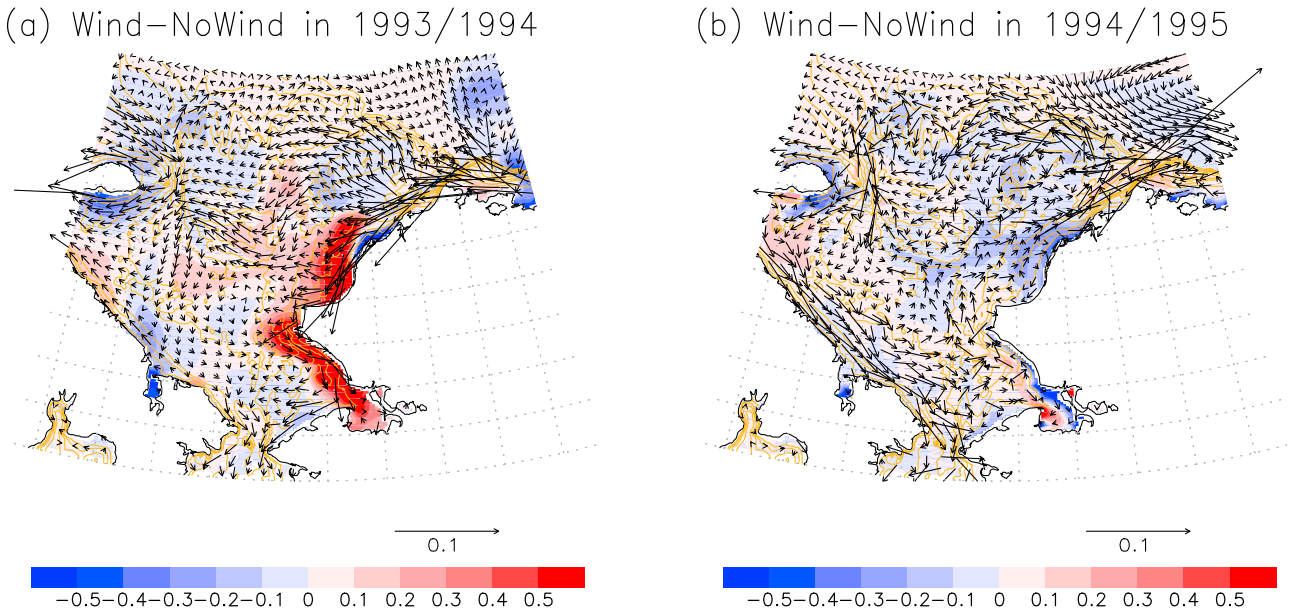

Figure 10. (a and b) Salinity and velocity differences between two experiments: with and without wind forcing. Values are averages over water columns in February.

[36] Thus, we believe that the model was sufficiently validated to discuss the movement and ventilation volume of the salt-enriched PWW.

5. Dense Water Formation and Transportation for Winters of 1993 and 1994

[37] Next, we discuss the dense water formation on the Chukchi shelf from the viewpoint of wind-driven circulation and salt-enriched water movement. For this purpose, we show the model results for typical winters with high and low ice production, namely, the winters of 1993/1994 and 1994/1995, respectively. The two winters have been examined based on the in situ observation on the Central Channel and the Hanna Shoal [*Weingartner et al.*, 2005; *Martin et al.*, 2004].

[38] The mooring observation [*Weingartner et al.*, 2005] indicates a drastic difference in the bottom salinity between the two winters. In the former winter, 1993/1994, extremely high saline water with S = 35.2 psu was found between December and February, which is equivalent to σ_θ = 28.3 kg m^{-3} corresponding to a density greater than that of the lower halocline layer (>200 m) in the Canada Basin. In contrast, they predominantly observed far less saline, cold winter water with S = 32.0–32.5 psu at the same locations in the next winter of 1994/1995. According to the SSM/I algorithm, the 1993/1994 winter exhibits the highest ice production among the 15 winters (1992–2006) (Figures 3a and 3b), as opposed to the 1994/1995 winter that exhibits the lowest ice production. Both *Weingartner et al.* [2005] and *Martin et al.* [2004] concluded that the large difference in ice production, expected from the SSM/I image, principally determines the difference in the observed salinity at the moorings. However, the oceanic circulation on the shelf must be considered because it can vary depending on winds, and consequently, influence the local salinity value through advection.

[39] Figure 7a and 7b show salinity distribution averaged for water columns during March in the winters of 1993/1994 and 1994/1995, respectively, where vertically averaged current is plotted in vector as well. The simulated salinity distribution is briefly outlined as follows. In the 1993 winter, high saline water is formed along the Alaskan coast, and then, it is advected northward along the three pathways. While, far less saline water is found in the winter of 1994, except for the high saline water within further limited coastal region.

[40] In November 1993, the broad areal ice production supplies a considerable amount of salt to the underlying shelf waters (Figure 8a). This leads to 0.3–0.7 psu salinity increase for the month in the broad shelf region, which additionally causes a salinity increase of ~1.5 psu per month in the coastal regions because of the frequent polynya formation there (Figure 9a). Using the mean salinity flux of F_s = 1–3 × 10^{-5} kg m s^{-1} observed for the month, a theoretical solution (7) (see Appendix) gives a salinity increase of 0.6–1.8 psu using H = 50 m, which is roughly consistent with the model results. In contrast, from December to January in the winter of 1993, quite intensive salinity inputs occurred along the western Alaskan coast; these were primarily caused by frequent polynya emergence associated with the strong northeasterly wind and they continued for nearly two months (Figure 8b). In mid-January, the Barrow polynya expanded over 100 km off the coast, and it partially covered the Central Channel and the Hanna Shoal. In these months, the northward oceanic flow, induced by the 0.8 Sv inflow, is considerably weakened on the shoals (Figure 9b), and there occurs a flow moving in the opposite direction. During these months, the salt provided at the surface remains on the shelf without draining the Barrow Canyon, and subsequently, the shelf water is imposed with the additional salt

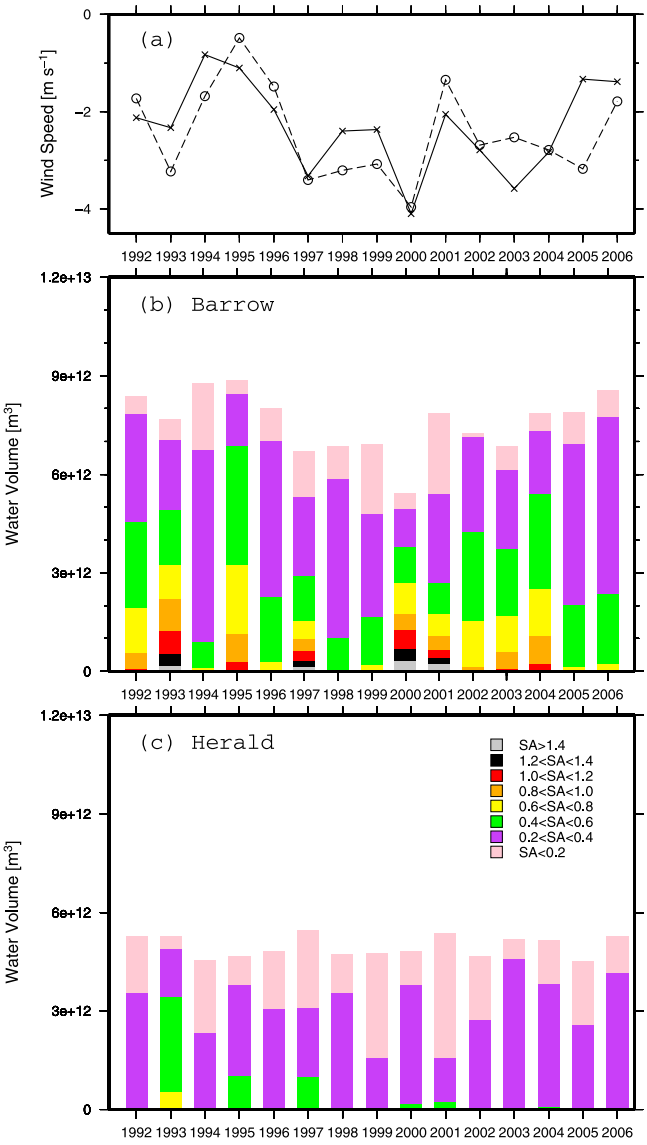

Figure 11. (a) Northward (dashed line with circle) and eastward (solid with cross) wind speed, where these are averages over the northern Chukchi Sea (69–72°N, 185–205°E) between November and May. Exiting water volume and salinity anomaly are shown for (b) Barrow and (c) Herald Valleys. These values are counted at corresponding sections in Figure 1.

input from further ice production. In reality, the reverse flow could be accompanied with the lift of saltier and warmer Atlantic origin basin water onto the shelf, so that the flow may have significantly contributed to the drastic salinity increase observed at the mooring stations in the 1993 winter.

[41] Ice production in the Alaskan polynyas occurs infrequently after March when steady northeasterly wind weakens (Figure 8c); this may be related to a gradual increase in air temperature. With the reduced ice production in spring, the strong mean flow caused by pressure gradient may mainly determine the salinity distribution. For example, during March in 1994, salinity rapidly increases by 0.6 psu to the west of Cape Lisburne because of saline water advection from the southern Chukchi Sea (Figure 9c) that propagates further northward in April.

[42] The simulation for the 1993 winter showed that the strong northeasterly wind attenuates the northward throughflow in December and January. To examine the effects of on-shelf circulation induced by the northeasterly wind on the dense water formation, we carried out additional experiments for the two winters. In the experiments, the model is forced merely by the external northward inflow with 0.8 Sv transport, where it is also applied with the same salinity flux at the surface in the absence of wind forcing.

[43] Figure 10a shows the difference in vertically averaged salinity and also current vectors between the two simulations for the end of February in 1994. Figure 10a shows that for the case with wind forcing, the salinity increase due to ice production is greatly intensified relative to that in the absence of wind forcing. In particular, the salinity enhancement is remarkable along the Alaskan coast between Icy Cape and Kotzebue Sound, being 0.7 psu at a maximum, whereas it is moderate in the Central Channel, being ~0.2 psu. This is interpreted that the northeasterly wind during the winter of 1993 promoted the salinity enhancement by prolonging the residence time of the water on the shelf and increasing opportunities to receive the salt input from ice production (refer to the discussion in the Appendix). In contrast, for the winter of 1994/1995 that is characterized by the weak northeasterly wind (Figure 10b), the effect of salinity enhancement because of the wind-driven circulation is not significant, although the northeastward Alaskan coastal current, draining into the Barrow Canyon, appears to be slightly enhanced.

6. Quantification of the Ventilation Water Volumes

[44] We attempt to quantify the ventilation volume at the cold halocline layer in the Canada Basin. First, we discuss the cumulative volumes of the exported water in the Barrow and Herald Canyons. Then, we show the results of the water remained on the Chukchi shelf by the end of spring because most of the waters left on the shelf until summer likely undergo warming and freshening [*Woodgate et al.*, 2005c].

6.1. Exported Water via Barrow and Herald Canyons

[45] Figure 11b shows the volume fluxes exported into the Canada Basin via the Barrow Canyon; the fluxes are computed at the section shown in Figure 1 and integrated for 7 months from November to May. Figure 11 indicates that the exported volume varies modestly over the years, with an average of 7.4×10^{12} m^3 and a standard deviation of 1.2×10^{12} m^3. As compared to the wind speed averaged for the same period (Figure 11a), the integrated water export is highly correlated with both the eastward and the northward wind speed (R = 0.88 and 0.78, respectively). In other words, it tends to be small in years in which a strong northeasterly wind blows along the Alaskan coast. For example, in the winters of 1997 and 2000, when a strong wind blows southwestward, the cumulative water volume is less than 7×10^{12} m^3.

[46] The maximum salinity increase and its volumetric ratio for the exported water are more variable; the maximum

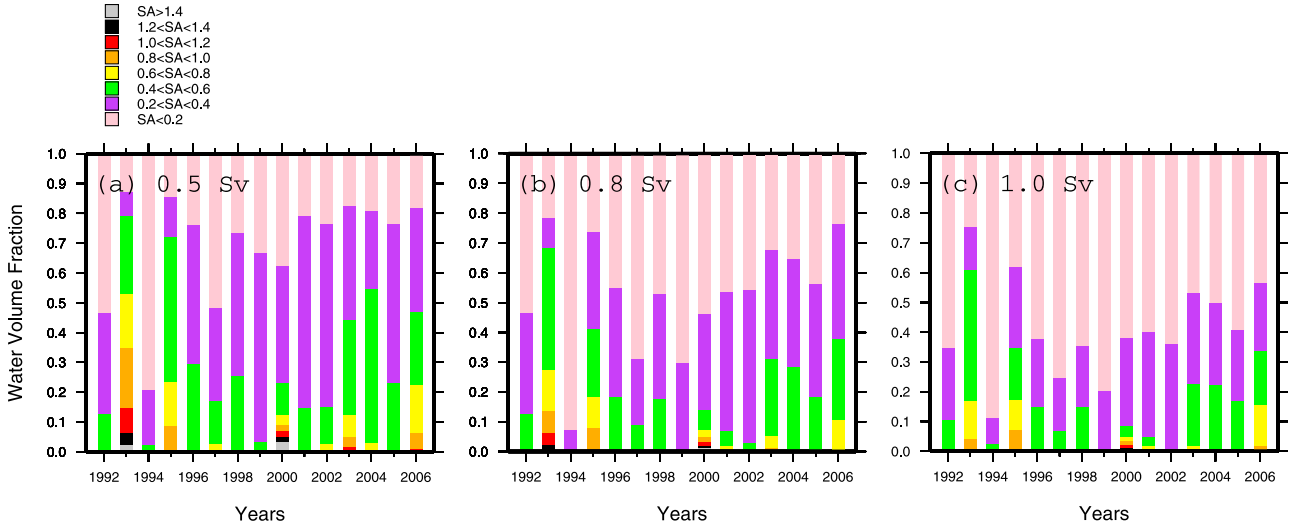

Figure 12. Volume and salinity anomaly of water remaining on the shelf at the end of May showing cases of inflowing rates for (a) 0.5, (b) 0.8, and (c) 1.0 Sv.

salinity increase is 0.6–1.7 psu, and it rarely exceeds 1.4 psu. Several winters such as 1993, 1995, 2000, and 2001 exhibited considerable occupancy of highly salt-enriched water (i.e., water with $\Delta S > 1.0$ psu occupies 20–30% of the overall volume). In particular, in the winter of 1993, 25% of the total volume was greatly enhanced to up to 0.9–2.2 psu. On the other hand, in the winters of 1994, 1998, 2005, and 2006, over 50% of the total volume is less saline than 0.4 psu anomalously.

[47] Next, the water exported via the Herald Valley is discussed (Figure 11c). The throughflow via the Herald Valley is relatively less variable in terms of both volume and salinity as compared to that via the Barrow Canyon. The salinity enhancement is quite characteristic and lies in a very narrow range of salinity anomaly, where roughly 75% of the waters are enhanced to as less as ~0.2 psu (an exception is the winter of 1993, when water with $\Delta S > 0.4$ psu occupies ~40% of the overall volume). This can be explained by fewer opportunities for salinity enhancement for the waters passing through the Herald Valley; these can be enriched by salt from Kotzebue polynya and in part from the Barrow polynya to the west of Pt. Hope in addition to the seasonal ice formation in the early winter.

6.2. Water Remaining on Chukchi Shelf Until Summer

[48] Next, we show the water volume and salinity anomaly for water remaining on the shelf until the end of May; the waters possibly undergo the warming and freshening associated with heat adoption because of solar radiation as mentioned. Expectedly, Figure 12b shows that the waters have a maximum salinity anomaly correlated with the wind strength along the Alaskan coast. For the winters of 1993 and 2000, some of the waters are highly salt enriched with $\Delta S > 1.4$ psu at a maximum; in both cases, the northeasterly wind is greater than 3 m s^{-1}. However, the maximum salinity anomaly of water remaining on the shelf tends to be lesser than that of water exiting from the shelf. For example, in the winter of 1997, the salinity of water remaining on the shelf is less than 0.6 psu, whereas that of the exiting water exceeds 1.4 psu. This implies that highly salt-enriched water ($\Delta S > 1.0$ psu) is effectively exported via the Barrow Canyon by the pressure gradient northward flow. In other words, the 0.8 Sv inflow sufficiently prevails over the reverse southward current induced by the northeasterly wind.

6.3. Sensitivity Test for Variation of Pressure Gradient Inflow

[49] *Woodgate et al.* [2005c] calculated the current velocity driven by the pressure gradient force in the Bering Strait and they reported that it is temporally variable by a factor of two. In the following, we examine how significantly the variable inflow from the Bering Strait can influence the exported water through the Barrow and Herald Canyons. Thus, we conducted another simulation with three inflowing rates, 0.5, 0.8 (default), and 1.0 Sv, at the Bering Strait (Figure 12). These experiments give a reasonable result in that the salt-enriched water is more effectively exported and disappears from the shelf when the prescribed inflow increases. This is most prominently observed for water with salinity anomaly of 0.2–0.5 psu; it occupies roughly 50% of the total shelf volume for the case of 0.5 Sv, whereas it occupied only ~20% for the case of 1.0 Sv.

[50] Table 2 shows the volume flux and salinity anomaly for each inflowing rate, where they are averaged for 15 years. The results show that the exports via both Barrow and Herald Canyons increase with the inflow rate from 0.36 to 0.62 Sv and from 0.25 to 0.36 Sv, respectively. Salinity across the Barrow Canyon does not respond significantly to a change in inflowing rate, where one forth of the overall volume has a salinity anomaly of 0.5–1.8 psu.

[51] In contrast, the water exported via the Herald Valley exhibits a clearer response to the variance in the inflowing rate. Twenty-five percent of the most saline water ranges in 0.3–0.7 psu, 0.2–0.5 psu, and 0.1–0.4 psu for 0.5, 0.8 and

Table 2. Mean Salinity and Transport via Barrow and Herald Canyons for Three Cases of Inflowing Rates, 0.5, 0.8 (default), and 1.0 Sv, From the Bering Strait[a]

	Barrow Canyon					Herald Valley				
	Transport (Sv)	Max ΔS (psu)	25%	50%	75%	Transport (Sv)	Max ΔS (psu)	25%	50%	75%
Case 1 (0.5 Sv)	0.36 [0.16]	1.7	0.5	0.4	0.2	0.25 [0.04]	0.7	0.3	0.1	0.1
Case 2 (0.8 Sv)	0.51 [0.14]	1.7	0.5	0.3	0.2	0.31 [0.06]	0.5	0.2	0.1	0.1
Case 3 (1.0 Sv)	0.62 [0.14]	1.8	0.5	0.3	0.2	0.36 [0.04]	0.4	0.1	0.1	0.1

[a]Values in brackets indicate the standard deviation for the exported water volume. The columns denoted as max ΔS, 25%, 50%, and 75% represent maximum value of salinity increase, and salinity increases (psu) at the accumulated water volumes from the maximum salinity.

1.0 Sv, respectively. In other words, the maximum salinity and the occupancy of highly saline water decrease with an increase of the inflow from the Bering Strait. This dependency of salinity across the Herald Valley can be understood from spatial pattern of a stream function ψ (Figure 13). Here, we show the result for the 2000 winter because it is the most illuminating case in which the northeasterly wind and the ice production in the Barrow polynya were the greatest among the 15 winters. When the external inflow is set to be 0.5 Sv, nearly all of the streamlines are directed northwestward to the west of Pt. Hope, indicating the drainage into the Herald Valley (as highlighted by thick contours). This is because northward passages such as the Central Channel and Alaskan Coastal Current cannot be established owing to the presence of a southwestward current induced by strong northeasterly wind in the northern shelf region (an area enclosed by blue line). These northwestward currents induced by the 0.5 Sv inflow transport most of brine-enriched water, which is formed associated with the Kotzebue polynya activity, toward the Herald Valley. Accordingly, the maximum salinity crossing the Herald Valley is considered to be higher. On the other hand, when the external inflow is intensified up to 0.8 Sv, the northward flow overcomes the reversal current caused by the northeasterly wind. Then, the pressure gradient flow carries the majority of highly brine-enriched water produced under the Kotzebue and Barrow polynya to the north. Consequently, the maximum salinity is reduced in the Herald Valley in the case with strong inflow.

7. Estimation of Real Range of Salinity

[52] Finally, we argue the practical range of salinity for the PWW exported into the Canada Basin. Because the present study starts the model calculation using spatially homogeneous salinity, the initial salinity value is a key parameter in determining the final salinity (density). We need to specify initial salinity to represent salinity when the seawater starts to freeze in the Chukchi Sea.

[53] The prescribed salinity is determined based on the moored measurements obtained by the University of Washington between 1990 and 2005 (see *Woodgate et al.* [2005b] for further information). Then, we chose the A3 site (65°N, 180°E), recommended by *Woodgate et al.* [2005b], which gives salinity appropriate for the Bering Strait. In Figure 14, the initial salinity is marked by a vertical line in each panel; it varies between 32.2 and 32.7 psu. To discuss the actual range of salinity, salinity anomaly calculated from the model is added to the prescribed initial value for each year.

[54] Figure 14 shows the actual salinity resulting from ice production, indicating the majority of which falls within the

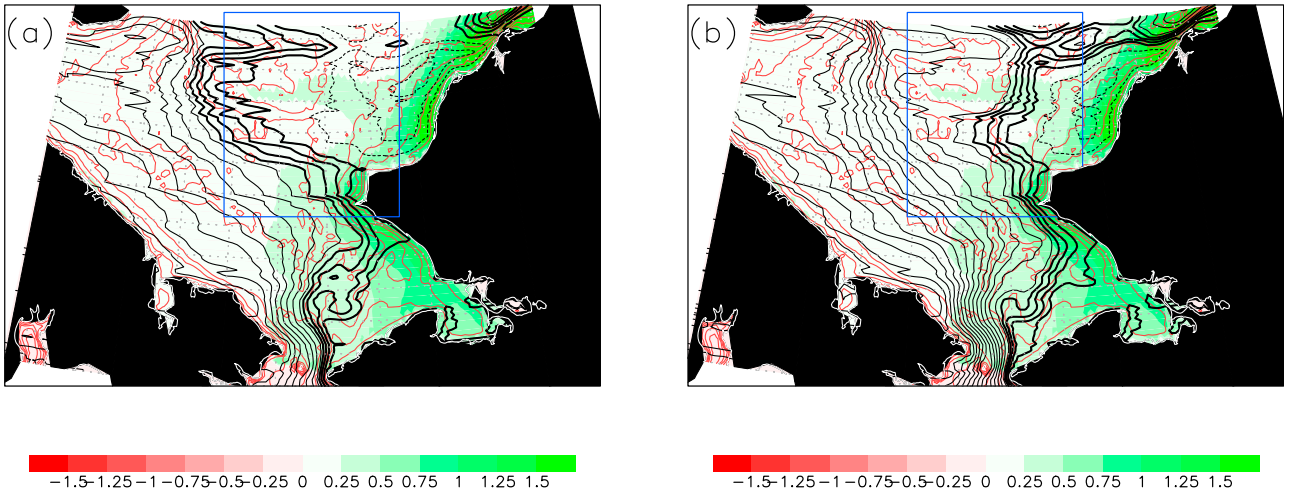

Figure 13. Mean stream function ψ for the winter of 2000, where external inflows with (a) 0.5 Sv and (b) 0.8 Sv are applied at southern boundary. Color indicates surface salinity flux ($\times 10^{-5}$ kg m s^{-1}) averaged for the winter. Streamline contours are 0.05 Sv. Pathways of waters to be focused are highlighted by thick contour in ψ and a region enclosed by blue lines.

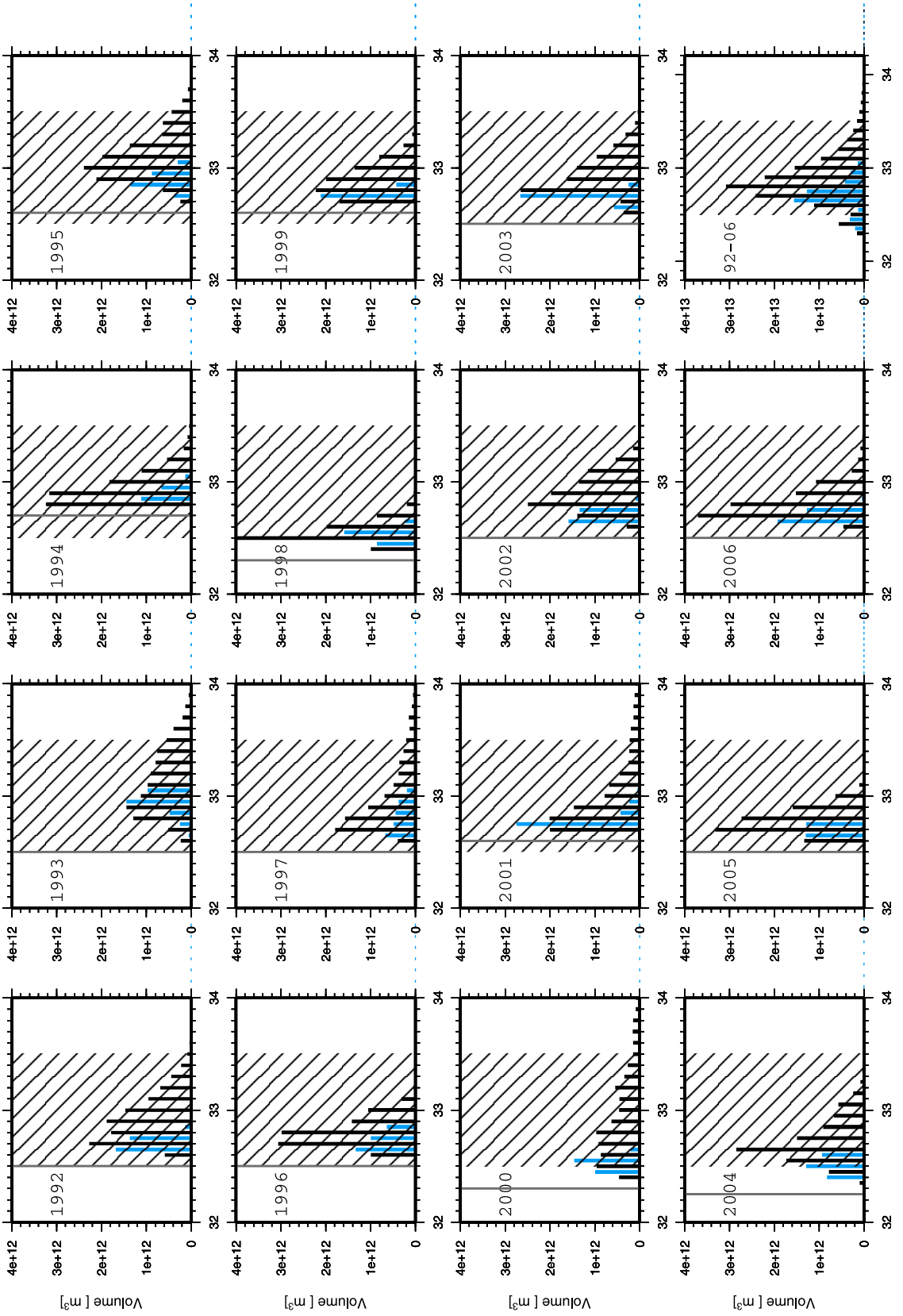

Figure 14. Accumulated water volumes exported via Barrow (bars in black) and Herald (bars in blue) Canyons, where salinity increment simulated is added to initial salinity prescribed based on mooring systems (denoted by vertical lines). Shaded region denotes a typical range of salinity for the cold halostad layer in Canada Basin.

shaded region of $S = 33.0 \pm 0.5$ psu, corresponding to the typical salinity of the cold halocline layer in the western Arctic Ocean [*Jones and Anderson*, 1986]. By accumulating the volumes of the salt-enhanced water (a panel in the right corner on bottom line), the salinity via the Barrow Canyon ranges in $S = 32.4$–33.8 psu with a peak of $S = 32.8$–32.9 psu, which is 0.2–0.3 psu smaller than 33.1 psu for the cold halocline layer. It is even smaller for the Herald Canyon, where the salinity ranges from $S = 32.6$–33.1 psu, although it has a similar peak of $S = 32.7$ psu that is similar to that for the Barrow Canyon.

[55] Integrating the water exports over the 15 years provides the following volumes: 110,000 km^3 via the Barrow Canyon and 33,000 km^3 via the Herald Valley, and these are converted to 0.24 and 0.07 Sv for the mean transports (accumulated volumes divided by 15 years). We have previously noted that major volume of the exiting water is less dense than the upper halocline layer with $S = 33.1$ psu, and therefore, it does not ventilate the layer in the basin. In order to achieve subduction into the depth, the shelf water needs to diapycnally mix with saltier deeper water [*Melling*, 1993; *Woodgate et al.*, 2005a]. If the diapycnal mixing is assumed, we can estimate the potential volume of the PWW to ventilate the cold halocline layer with $S = 33.1$ psu. Here, we assume a single prescribed salinity, as done by *Winsor and Björk* [2000] and *Cavalieri and Martin* [1994] in that they chose $S = 32.85$ psu for the value based on the theoretical estimate of *Björk* [1989, 1990]. In this study, we adopt $S = 34.0$ psu assuming that if the water is less saline than $S = 33.1$ psu, it mixes with the lower halocline layer water. In addition, for water saltier than 33.1 psu, we assume mixture with waters of $S = 32.0$ psu, corresponding to salinity in the surface mixed layer lying above the cold halostad layer. This estimation is based on the following formulation [cf. *Cavalieri and Martin*, 1994]:

$$V_H = \begin{cases} V_D(S - 34.0)/(33.1 - 34.0) & S < 33.1, \\ V_D(S - 32.0)/(33.1 - 32.0) & S > 33.1, \end{cases} \quad (2)$$

where V_D is the volume of dense water using $S = S_w + \Delta S$, where S_w is the initial salinity and ΔS the salinity anomaly obtained from the model calculation, while V_H is the volume of water with $S = 33.1$ psu. This calculation gives an annual average of the potential ventilation volume via the Barrow and Herald Canyons as 14,800 km^3 and 5,000 km^3 (0.31 and 0.10 Sv for the mean transport), respectively. This value is 35% of the theoretical estimate of 1.2 Sv [*Björk*, 1990] that maintains the cold halocline layer in the Arctic Ocean. This assumption also enables us to have a rough estimate of the renewal time of the cold halocline layer in the Canada Basin. If the entire volume of such layer is approximated to be 1.6–2.4×10^5 km^3 (100–150 m thickness multiplied by an area of Canada Basin, 1.6×10^6 km^2), the renewal time should be about 4–6 years. This value agrees well with 4.3 ± 1.7 years presented by *Ekwurzel et al.* [2001] based on the mean age of ^{3}H-^{3}H$_e$.

8. Summary

[56] In the present study, dense water formation resulting from ice production is examined on the Chukchi shelf, where a three-dimensional primitive equation ocean model is adopted with realistic bathymetry. The model is forced by NCEP wind and imposed with the surface salinity flux calculated using the SSM/I thin ice thickness algorithm.

[57] First, we conducted a brief analysis of ice production in the Chukchi Sea using the data derived from the SSM/I algorithm. The SSM/I satellite showed that the Barrow coastal polynya favorably opens for a strong easterly or northeasterly wind. According to the model calculation, such wind weakens the northward throughflow driven by pressure head forcing, resulting in a reduction in the water export from the Barrow Canyon. In some winters with strong winds, e.g., 1993 and 2000, the salinity increase in the exported water was remarkably high. In contrast, in winters with weak winds, most of the exported water had low salinity (<0.5 psu) because of reduced occurrence of Barrow coastal polynya. An idealized experiment in the absence of wind forcing shows that the water export via the Barrow Canyon is greatly restricted by the strong northeasterly wind, and therefore a portion of the shelf water remains on the shelf along the Alaskan coast; this water then undergoes further salinity enhancement from the Alaskan coastal polynyas.

[58] With respect to the throughflow via Herald Valley, the exported water is substantially small in volume and salinity enhancement, these being roughly 0.3 Sv and 0.1–0.2 psu, respectively. In addition, the variables are both less sensitive to the strength of the northeasterly wind, unlike the case in the Barrow Canyon.

[59] The model also shows that the throughflow via the Herald Valley is dependent on the strength of the external inflow from the southern boundary. As a result, the maximum salinity across the Herald Valley decreases with an increase of inflowing rate from Bering Strait. This can be explained by the fact that the northward flow induced by the pressure gradient force overcomes southwestward current induced by the northeasterly wind, following which the salt-enriched water beneath the Kotzebue polynya penetrates northward and avoids entering the Herald Valley.

[60] According to the simulations of the 15 year period and the moored salinity at the Bering Strait, the salinity across the Barrow and Herald Canyons is 32.9 ± 0.8 psu and 32.7 ± 0.3 psu, respectively; these values are slightly lower than $S = 33.1$ psu that is typically observed in the Canada Basin. The above estimation also gives the subduction rates of the PWW via the Barrow and Herald Canyons as 0.2 and 0.07 Sv, respectively. Considering the diapycnal mixing with the lower halocline layer water and the surface mixed layer water gives mean ventilation volumes of 0.3 and 0.1 Sv at the cold halocline layer with $S = 33.1$ psu.

Appendix A: Theory for Salinity Determination on the Shelf

[61] Formulations on salinity budget would be instructive in understanding salinity change on the shelf. The local salinity is defined as the sum of initial salinity $S_0(x, y)$ and its temporal variation $S'(x, y, t)$ that is further decomposed by long-term average and eddy component, respectively

denoted by $\overline{S}(x, y, t)$ and $S''(x, y, t)$. The local salinity change is written as follows:

$$\frac{\partial}{\partial t}\left(S_0 + \overline{S} + S''\right) = \nabla \cdot \left((\mathbf{u_0} + \mathbf{u}')\left(S_0 + \overline{S} + S''\right)\right) + F_s/h, \quad \text{(A1)}$$

where $F_s(x, y, t)$ is the salinity flux due to ice production, and $h(x, y)$ is the bottom topography. If all of the terms in equation (A1) are integrated over an arbitrary period of time longer than timescale associated with eddy development, i.e., >∼10 days, all terms multiplied by a fluctuation become zero, giving

$$\frac{\partial \overline{S}}{\partial t} = \sum_{n=1}^{2} \frac{\partial}{\partial x}\left(u_{0n}S_0 + u_{0n}\overline{S} + u_n'S''\right) + F_s/h, \quad \text{(A2)}$$

where the subscripts n = 1 and 2 denote the x and y directions, respectively. By introducing stream function $\psi(t, \ell)$, defined to be $-\mathbf{k} \times \nabla\psi = \mathbf{u_0}$, (4) can be rewritten in terms of distance ℓ from an arbitrary location along the streamline.

[62] Under the presence of coastal-trapped circulation, baroclinic eddies for the polynya problem are significantly attenuated because the density front is affected by the current before it becomes unstable [*Chapman*, 2000; *Kawaguchi and Mitsudera*, 2009]. Thus, if the salinity flux associated with eddies, i.e., $u'S''$ in (4), is neglected, and also the background salinity is assumed to be homogeneous (∇S_0 = 0), equation (A2) becomes

$$\frac{\partial \overline{S}}{\partial t} = u_0 \frac{\partial \overline{S}}{\partial \ell} + F_s/h. \quad \text{(A3)}$$

Equation (A3) is then solved as follows:

$$\overline{S}(t, \ell_0) = \int^{\ell_0} F_s/(u_0 h)d\ell = \int^{\ell_0} F_s/(\mathbf{k} \times \nabla\psi)d\ell. \quad \text{(A4)}$$

Alternatively, it is solved in the Lagrangian form as

$$\overline{S}(t) = \int^{\ell_0/u_0} F_s/h dt. \quad \text{(A5)}$$

This shows that local salinity is determined by both surface salinity flux and lateral current along the streamline, suggesting the importance of passage and current strength of the Pacific water.

[63] **Acknowledgments.** The authors thank K. Shimada of the Tokyo University for Marine Science for his instructive comments and helpful discussion. We also sincerely acknowledge the two anonymous reviewers and the Associate Editor for their valuable comments and suggestions. The SSM/I and AVHRR data were provided by the National Snow and Ice Data Center (NSIDC), University of Colorado. This work was supported by the fund from Core Research for Evolutional Science and Technology of Japan Science and Technology Agency and from grant-in-aids for scientific research (20221001) of the Japanese Ministry of Education, Culture, Sports, Science and Technology.

References

Aagaard, K., L. K. Coachman, and E. Carmack (1981), On the halocline of the Arctic Ocean, *Deep Sea Res., Part A*, *28*, 28,529–28,545.

Björk, G. (1989), A one-dimensional time-dependent model for the vertical stratification of the upper Arctic Ocean, *J. Phys. Oceanogr.*, *19*(1), 52–67.

Björk, G. (1990), The vertical-distribution of nutrients and O-18 in the upper Arctic-Ocean, *J. Geophys. Res.*, *95*, 16,025–16,036.

Blumberg, A. F., and G. L. Mellor (1987), A description of a three dimensional coastal ocean circulation model, in *Three-Dimensional Coastal Ocean Model*, *Coastal Estuarine Sci.*, vol. 4, edited by N. S. Heaps, pp. 1–16, AGU, Washington, D. C.

Cavalieri, D. J., and S. Martin (1994), The contribution of Alaskan, Siberian, and Canadian coastal polynyas to the cold halocline layer of the Arctic Ocean, *J. Geophys. Res.*, *99*, 18,343–18,362.

Chapman, D. C. (2000), The influence of an alongshore current on the formation and offshore transport of dense water from a coastal polynya, *J. Geophys. Res.*, *105*, 24,007–24,019.

Comiso, J. C. (1986), Characteristics of Arctic winter sea ice from satellite multispectral microwave observations, *J. Geophys. Res.*, *91*, 975–994.

Comiso, J. C., S. F. Ackley, and A. L. Gordon (1984), Antarctic sea ice microwave signatures and their correlation with in situ ice observations, *J. Geophys. Res.*, *89*, 662–672.

Drucker, R., S. Martin, and R. Moritz (2003), Observations of ice thickness and frazil ice in the St. Lawrence Island polynya from satellite imagery, upward looking sonar, and salinity/temperature moorings, *J. Geophys. Res.*, *108*(C5), 3149, doi:10.1029/2001JC001213.

Ekwurzel, B., P. Schlosser, R. A. Mortlock, R. G. Fairbanks, and J. Swift (2001), River runoff, sea ice meltwater, and Pacific water distribution and mean residence timesin the Arctic Ocean, *J. Geophys. Res.*, *106*, 9075–9092.

Jones, E. P., and L. G. Anderson (1986), On the origin of the chemical properties of the Arctic Ocean halocline, *J. Geophys. Res.*, *91*, 10,759–10,767.

Kawaguchi, Y., and H. Mitsudera (2009), Effects of along-shore wind on DSW formation beneath coastal polynyas: Application to the Sea of Okhotsk, *J. Geophys. Res.*, *114*, C10013, doi:10.1029/2008JC005041.

Kawaguchi, Y., S. Nihashi, H. Mitsudera, and K. I. Ohshima (2010), Formation mechanism of huge coastal polynyas and its application to Okhotsk northwestern polynya, *J. Phys. Oceanogr.*, *40*, 2451–2465.

Kwok, R. (2008), Summer sea ice motion from the 18 GHz channel of AMSR-E and the exchange of sea ice between the Pacific and Atlantic sectors, *Geophys. Res. Lett.*, *35*, L03504, doi:10.1029/2007GL032692.

Martin, S., and P. Kaufman (1981), A field and laboratory study of wave damping by grease ice, *J. Glaciol.*, *27*, 283–314.

Martin, S., R. Drucker, and K. Yamashita (1998), The production of ice and dense shelf water in the Okhotsk Sea polynyas, *J. Geophys. Res.*, *103*, 27,771–27,782.

Martin, S., R. Drucker, R. Kwok, and B. Holt (2004), Estimation of the thin ice thickness and heat flux for the Chukchi Sea Alaskan coast polynya from Special Sensor Microwave/Imager data, 1990–2001, *J. Geophys. Res.*, *109*, C10012, doi:10.1029/2004JC002428.

Melling, H. (1993), The formation of a haline shelf front in wintertime in an ice-covered Arctic Sea, *Cont. Shelf Res.*, *13*, 1123–1147.

Pease, C. (1987), The size of wind-driven coastal polynyas, *J. Geophys. Res.*, *92*, 7049–7059.

Rigor, I. G., J. M Wallace, and R. L. Colony (2002), Response of sea ice to the arctic oscillation, *J. Clim.*, *15*, 2648–2663.

Rothrock, D. A., R. Kwok, and D. Groves (2000), Satellite views of the Arctic Ocean freshwater balance, *The Freshwater Budget of the Arctic Ocean*, edited by E. L. Lewis, pp. 409–452, Kulwer Acad., Dordrecht, Netherlands.

Shimada, K., M. Itoh, S. Nishino, F. McLaughlin, E. Carmack, and A. Proshutinsky (2005), Halocline structure in the Canada Basin of the Arctic Ocean, *Geophys. Res. Lett.*, *32*, L03605, doi:10.1029/2004GL021358.

Shimada, K., T. Kamoshida, M. Itoh, S. Nishino, E. Carmack, F. A. McLaughlin, S. Zimmermann, and A. Proshutinsky (2006), Pacific Ocean inflow: Influence on catastrophic reduction of sea ice cover in the Arctic Ocean, *Geophys. Res. Lett.*, *33*, L08605, doi:10.1029/2005GL025624.

Stroeve, J., M. M. Holland, W. Meier, T. Scambos, and M. Serreze (2007), Arctic sea ice decline: Faster than forecast, *Geophys. Res. Lett.*, *34*, L09501, doi:10.1029/2007GL029703.

Tamura, T., and K. I. Ohshima (2011), Mapping of sea ice production in the Arctic coastal polynyas, *J. Geophys. Res.*, doi:10.1029/2010JC006586, in press.

Tamura, T., K. I. Ohshima, H. Enomoto, K. Tateyama, A. Muto, S. Ushio, and R. A. Massom (2006), Estimation of thin sea-ice thickness from NOAA AVHRR data in a polynya of the Wilkes Land coast, East Antarctica, *Ann. Glaciol.*, *44*, 269–274.

Tamura, T., K. I. Ohshima, T. Markus, D. J. Cavalieri, S. Nihashi, and N. Hirasawa (2007), Estimation of thin ice thickness and detection of fast ice from SSM/I data in the Antarctic Ocean, *J. Atmos. Oceanic Technol.*, *24*, 1757–1772.

Tamura, T., K. I. Ohshima, and S. Nihashi (2008), Mapping of sea ice production for Antarctic coastal polynyas, *Geophys. Res. Lett.*, *35*, L07606, doi: 10.1029/2007GL032903.

Walsh, J. J., et al. (1989), Carbon and nitrogen cycling within the Bering/Chukchi seas: Source regions for organic matter effecting AOU demands of the Arctic Ocean, *Prog. Oceanogr.*, *22*, 259–277, doi:10.1016/0079-661(89)90006-2.

Weingartner, T. J., D. J. Cavalieri, K. Aagaard, and Y. Sasaki (1998), Circulation, dense water formation, and outflow on the northeast Chukchi shelf, *J. Geophys. Res.*, *103*, 7647–7661.

Weingartner, T. J., S. L. Danielson, and T. C. Royer (2005), Freshwater variability and predictability in the Alaska Coastal Current, *Deep Sea Res., Part II*, *52*, 169–191, doi:110.1016/j.dsr1012.2004.1009.1030.

Winsor, P., and G. Björk (2000), Polynya activity in the Arctic Ocean from 1958 to 1997, *J. Geophys. Res.*, *105*, 8789–8803.

Winsor, P., and D. C. Chapman (2002), Distribution and interannual variability of dense water production from coastal polynyas on the Chukchi shelf, *J. Geophys. Res.*, *107*(C7), 3079, doi:10.1029/2001JC000984.

Winsor, P., and D. C. Chapman (2004), Pathways of Pacific water across the Chukchi Sea: A numerical model study, *J. Geophys. Res.*, *109*, C03002, doi:10.1029/2003JC001962.

Woodgate, R. A., K. Aagaard, J. H. Swift, K. K. Falkner, and W. M. Smethie Jr. (2005a), Pacific ventilation of the Arctic Ocean lower halocline by upwelling and diapycnal mixing over the continental margin, *Geophys. Res. Lett.*, *32*, L18609, doi:10.1029/2005GL023999.

Woodgate, R. A., K. Aagaard, and T. J. Weingartner (2005b), Monthly temperature, salinity, and transport variability of the Bering Strait through flow, *Geophys. Res. Lett.*, *32*, L04601, doi:10.1029/2004GL021880.

Woodgate, R. A., K. Aagaard, and T. J. Weingartner (2005c), A year in the physical oceanography of the Chukchi Sea: Moored measurements from autumn 1990–1991, *Deep Sea Res., Part II*, *52*, 3116–3149, doi:10.1016/j.dsr2.2005.10.016.

Yu, Y., and D. A. Rothrock (1996), Thin ice thickness from satellite thermal imagery, *J. Geophys. Res.*, *101*, 25,753–25,766.

M. Itoh, Y. Kawaguchi, T. Kikuchi, and S. Nishino, Japan Agency for Marine-Earth Science and Technology, 2-15, Natsushima-cho, Yokosuka 237-0061, Japan. (yusuke.kawaguchi@jamstec.go.jp)

H. Mitsudera, Institute of Low Temperature Science, Hokkaido University, Sapporo 060-0819, Japan.

T. Tamura, Antarctic Climate and Ecosystem Cooperative Research Center, University of Tasmania, Hobart, Tas. 7001, Australia.